ELSEVIER

Journal of Atmospheric and Solar-Terrestrial Physics 66 (2004) 1271–1282

Journal of ATMOSPHERIC AND SOLAR-TERRESTRIAL PHYSICS

www.elsevier.com/locate/jastp

Observational evidence for velocity convergence toward magnetic neutral lines as a factor in CME initiation

Yan Li*, Janet Luhmann, George Fisher, Brian Welsch

Space Sciences Laboratory, 7 Gauss Way, University of California, Berkeley, CA 94720-7450, USA

Received 5 February 2004; received in revised form 19 March 2004; accepted 30 March 2004
Available online 14 August 2004

Abstract

One of the major challenges of space weather research and modeling is the identification of the mechanism(s) for coronal mass ejections (CMEs). A leading candidate tested in several recent numerical simulations is photospheric magnetic flux cancellation by velocity convergence toward the neutral line of an active region having sheared or twisted magnetic fields. These attributes have been assumed in various combinations in modeling studies, but little observational work has been done that demonstrates their presence. In this paper, we show observational evidence that this process is at work in two different types of repetitively eruptive active regions in late 1996 and early 1997. The horizontal velocity field is obtained by applying Local Correlation Tracking (LCT) technique to sequences of photospheric line-of-sight magnetograms.

Keywords: Magnetogram; LCT; Coronal mass ejections; Space weather

1. Introduction

The question of what physical process or processes produce coronal mass ejections (CMEs) has inspired much of the recent space weather research on the solar end of the coupled Sun–Earth system. Energy storage models are the most widely accepted candidates because they are most consistent with observations suggesting the involvement of twisted or sheared magnetic fields that have relatively long lifetimes (e.g. Linker et al., 2003). Indeed, many modelers have focused on determining the physics needed to produce active region field lines that look like the sigmoidal soft X-ray loops identified as CME precursors by Canfield et al. (1999), with the expectation that CME initiation insights might follow.

Numerical simulations in turn have demonstrated that sigmoidal field structures can be produced in a number of ways. They can simply emerge as twisted S-shaped flux ropes from beneath the photosphere (e.g., Magara and Longcope, 2001; Fan, 2001; Magara, 2001) which possess S-shaped field lines within them that may become heated to X-ray temperatures during the rope's evolution in the coronal atmosphere (e.g., Fan and Gibson, 2003), or they can be produced by subjecting the footpoints of untwisted active region coronal arcades to combinations of vortical motions (e.g. Amari et al., 2003a; Lionello et al., 2002; Tokman and Bellan, 2002; Roussev et al., 2004). Amari et al. (2003a) further illustrate that an additional motion consisting of convergence toward the neutral line, which effectively produces magnetic flux cancellation at the photosphere (Linker et al., 2001, 2003), results in eruption of the

*Corresponding author. Tel.: +1 510-643-1559; fax: +1 510-643-8302

E-mail address: yanli@ssl.berkeley.edu (Yan Li).

1364-6826/$ - see front matter © 2004 Elsevier Ltd. All rights reserved.
doi:10.1016/j.jastp.2004.03.017

sigmoidal structure. This bulk convergence can be replaced by diffusive motion-related cancellation at the neutral line with a similar effect (Amari et al., 2003b). As sigmoids themselves can be quite stable for a number of solar rotations, the converging and/or diffusive flows toward the neutral line are a critical aspect of the process that one expects to find in at least some eruptive active region sites. Individual case studies of the photospheric magnetic field morphology and evolution prior to and during CMEs have been carried out for many years. One often cited result is that emergence of new magnetic flux with the opposite polarity of the existing active region flux occurs at the time of CME initiations (Feynman and Martin, 1995). Wang (2001) has pointed out that rearrangement of the active region coronal field connections by the introduction of new photospheric fields in such cases can destroy the magnetic topology, leading to the disappearance, by either eruption or collapse, of the magnetically suspended filament. The implication is that a CME accompanies the filament eruptions. However, often there is little or no special photospheric magnetic field change in the involved active region or connected regions accompanying a CME, even though a low coronal flare and/or filament eruption may occur. Instead, the active region appears to evolve smoothly through the eruption by either apparent photospheric motions or by flux emergence and cancellation. In some of these examples the erupting active region includes a rotating sunspot (e.g. Brown et al., 2003). However, in all such cases one cannot identify an obvious time of the CME by examining the photospheric field only.

In this study, we use time sequences of SOHO/MDI magnetograms obtained during a series of filament eruption-related CMEs in a decaying active region in late 1996, and a period of flare-related CMEs in May 1997 to illustrate that transverse velocities inferred by local correlation tracking (LCT) methods support the idea that velocity convergence toward the magnetic neutral line is a common property of the motions in eruptive regions. The combination of shearing motion and velocity convergence and/or diffusion toward the neutral line that characterizes the eruption mechanism of Amari et al. (2003a, b) may be at work. We suggest how LCT may be useful in specifying the boundary conditions for simulating CME eruptions in magnetogram-based coronal MHD models.

2. Description of the period of interest

2.1. Active region 7978 in 1996

The long-lasting NOAA active region 7978 first emerged on July 4, 1996 at S10 E31 during solar minimum and was the only or dominant activity center on the Sun during its life span. AR7978 produced one x-flare soon after and many smaller flares (Hudson et al., 1998) in its early phase of life. The region, which manifested the old cycle magnetic polarity (its leading field polarity was opposite to the polar field in the southern hemisphere), continued to be active during 5 rotations, producing many CMEs (Démoulin et al., 2002; Luhmann et al., 2003). During the evolution of the region, filaments formed at the magnetic neutral line, and repeatedly disappeared (usually partially) and reformed. During the extended decay phase, when the active region took on the appearance in magnetograms of a large, diffuse, sheared bipolar region, a long filament was seen along the neutral line. The long filament disappeared at the very end of the day September 25, 1996. A Halo CME was first observed by LASCO/C2 at 5:05UT on September 26, expanding at a slow speed of about 200 km/s. The filament seemed to be slowly reforming in the same channel after the eruption, but only a small part of the filament was formed before the region rotated to the backside on September 30. When the region came back to the east limb, the filament appeared to be fully reformed. On October 19 in the following rotation, the reformed filament disappeared again when the region was about 45° east of the disk center. It then took two days for the filament to reform to a similar state in the same channel and continued to build up in volume during the disk passage. No filament disappearance was seen before the region rotated to the back of the Sun on October 30. Fig. 1 shows a selection of SOHO/MDI magnetograms and BBSO Hα images that illustrate part of the above sequence of events, and the characteristics of this repeatedly erupting region.

For our study we elected to focus on the specific period at the end of September when a period of high cadence (2 min temporal resolution) MDI magnetograms was available. These observations will be further described below. The selected period was typical of the decaying phase of AR7978 and included the slow CME on September 26 associated with the filament eruption at the end of September 25.

2.2. Active region 8038 in May 1997

NOAA active region 8038 emerged on the back of the Sun and appeared on the east limb at N21 on May 4, 1997. Initially this active region exhibited the magnetic polarity pattern of the prevailing cycle. A flare and a classic three-part limb CME occurred on May 5. The region continued to be active as it crossed the disk. A flare and a Halo CME occurred around 5:00 UT on May 12, 1997 when the active region was at N21W08 slightly west of the disk center. This event was the focus of many studies because it was isolated on a magnetically simple disk and yet exhibited all of the interesting solar and

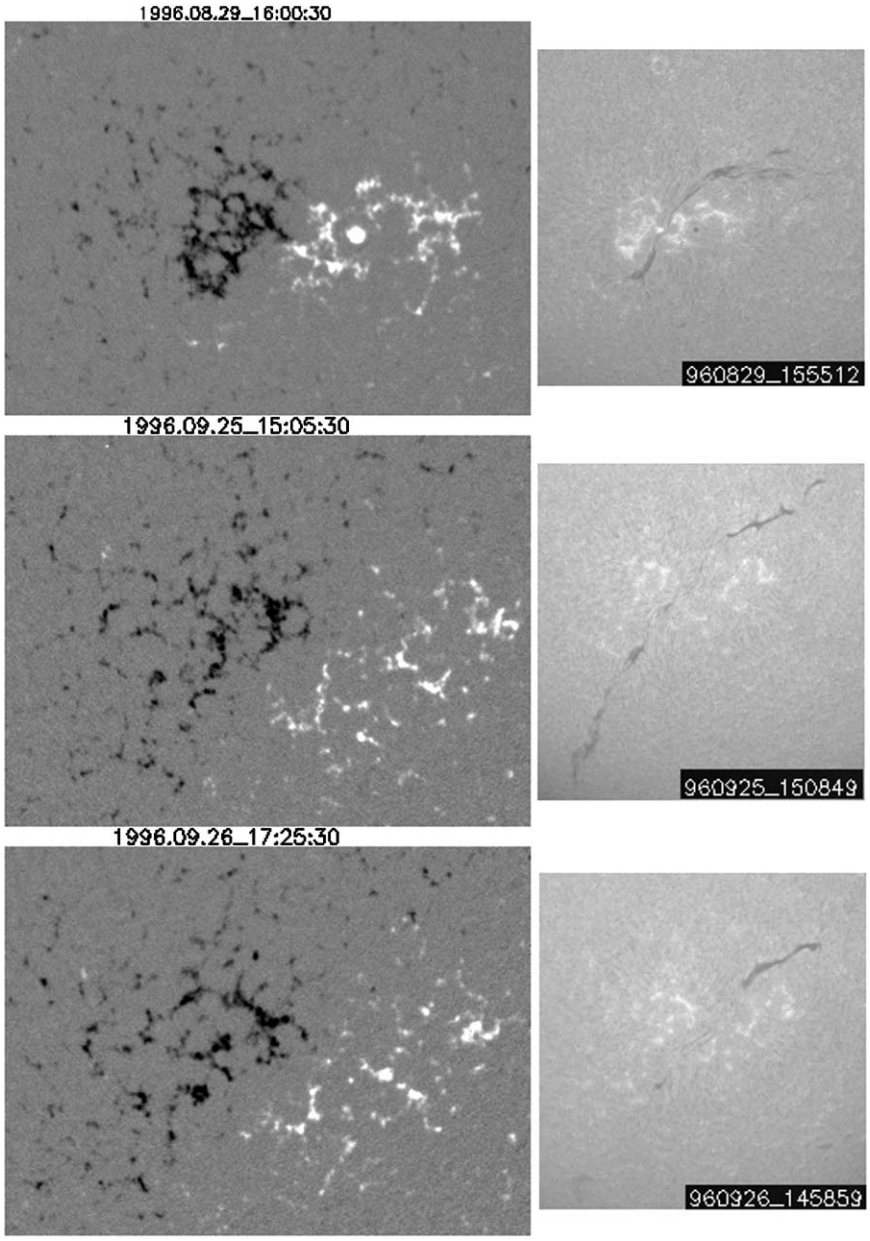

Fig. 1. A selection of SOHO/MDI magnetograms (left) and BBSO Hα images (right) that illustrate part of the above sequence of events, and the characteristics of this repeatedly erupting region.

interplanetary features of a space weather event. In particular, the flare was followed by or accompanied by a nearly circular wave centered on the active region, and by double dimmings flanking it in the SOHO/EIT images (Thompson et al., 1998). Webb et al. (2000) interpreted the double dimmings as the footprints of the coronal loop that had expanded to form the CME. There was also an SXT sigmoid over the active region, which apparently erupted with the event and was replaced by a post flare/CME arcade that had no twist and appeared to agree with potential field topology. The sigmoid then reformed and another eruption took place on May 16 near the limb, again with a flare and a three-part limb CME. With all three CMEs, some SXT arcades that appear to have the form of potential fields connect the active region to both the edge of the north polar coronal hole and the southern hemisphere. Fig. 2 presents a series of YOHKOH/SXT images over the disk passage.

Active region 8038 remained quite compact throughout its disk passage. It included a nearly circular positive

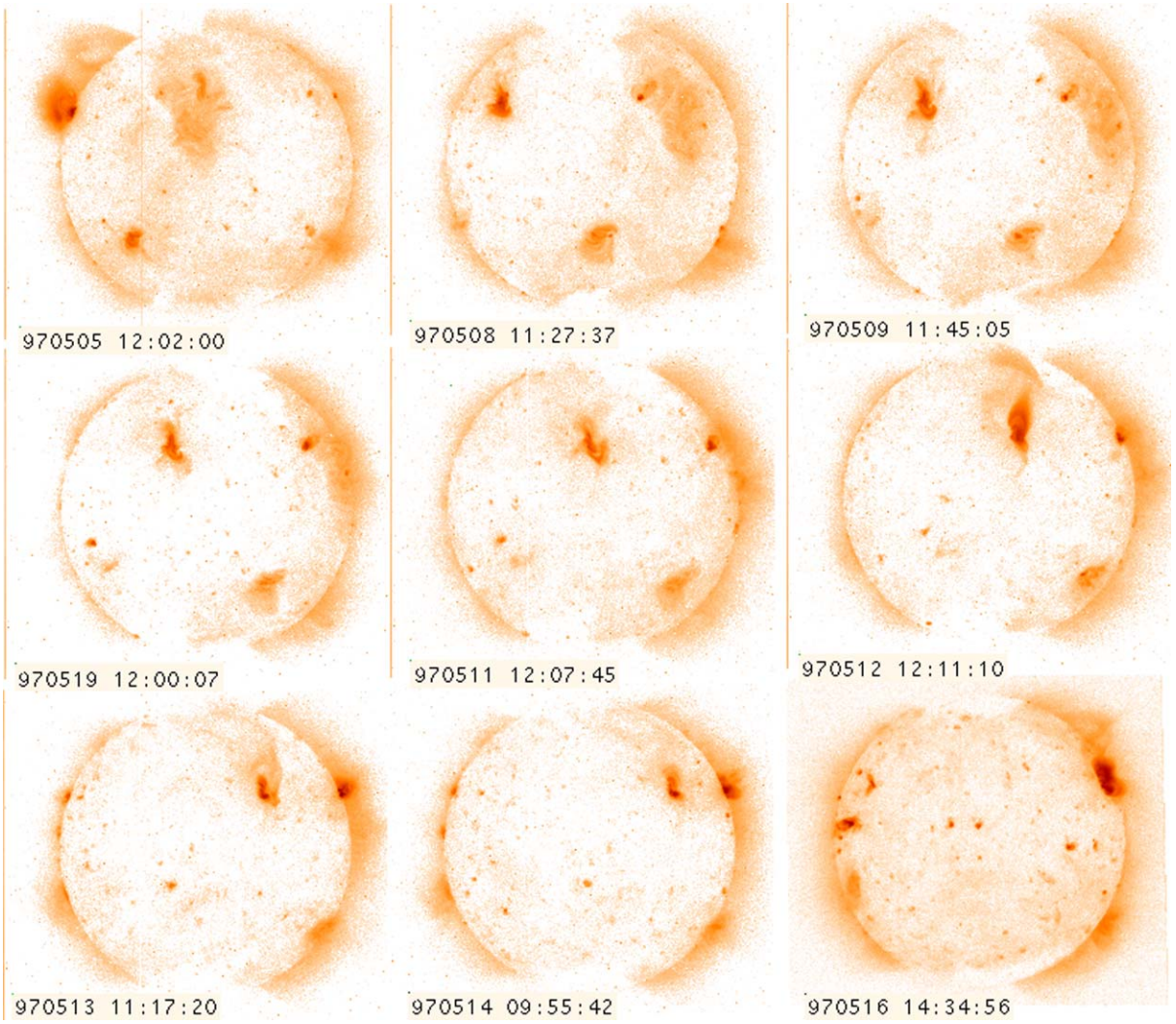

Fig. 2. A series of YOHKOH/SXT images over the disk passage during May 6 to 16, 1997. There were three CMEs with flares on May 5, 12 and 16.

polarity sunspot in its initially leading portion, and a diffuse negative polarity region that originally trailed the spot. Fig. 3 shows a time-lapse sequence of the evolution of this active region from limb to limb as seen with the SOHO/MDI magnetograph and BBSO Hα images. As the region crossed the disk the diffuse negative polarity region appeared to migrate toward and around the positive spot. The filament along the neutral line was sometimes rather fragmentary but seemed to persist as the magnetic field distribution of the active region changed. It is notable that even though the polarity distribution changed significantly across the disk, each of the three CMEs on May 5, 12 and 16 associated with this region showed similar features such as the polar-connected loops in the SXT images during and following the eruptions. Nightingale (2003 pers. comm.) has reported rotation in the sunspot of active region 8038 around the time of the May 12 CME. The period we analyze here is also around the time of the May 12 eruption with the active region near the central disk, when the highest quality magnetogram observations for this region were available.

3. LCT method applied to magnetogram data sets

Our goal is to determine whether velocity convergence toward the active region magnetic neutral line, such as that assumed in the initiation of simulated CMEs by Amari et al. (2003a, b), Tokman and Bellan (2002), and Linker et al. (2001) is present during the above periods of observed repeating events. Local correlation tracking,

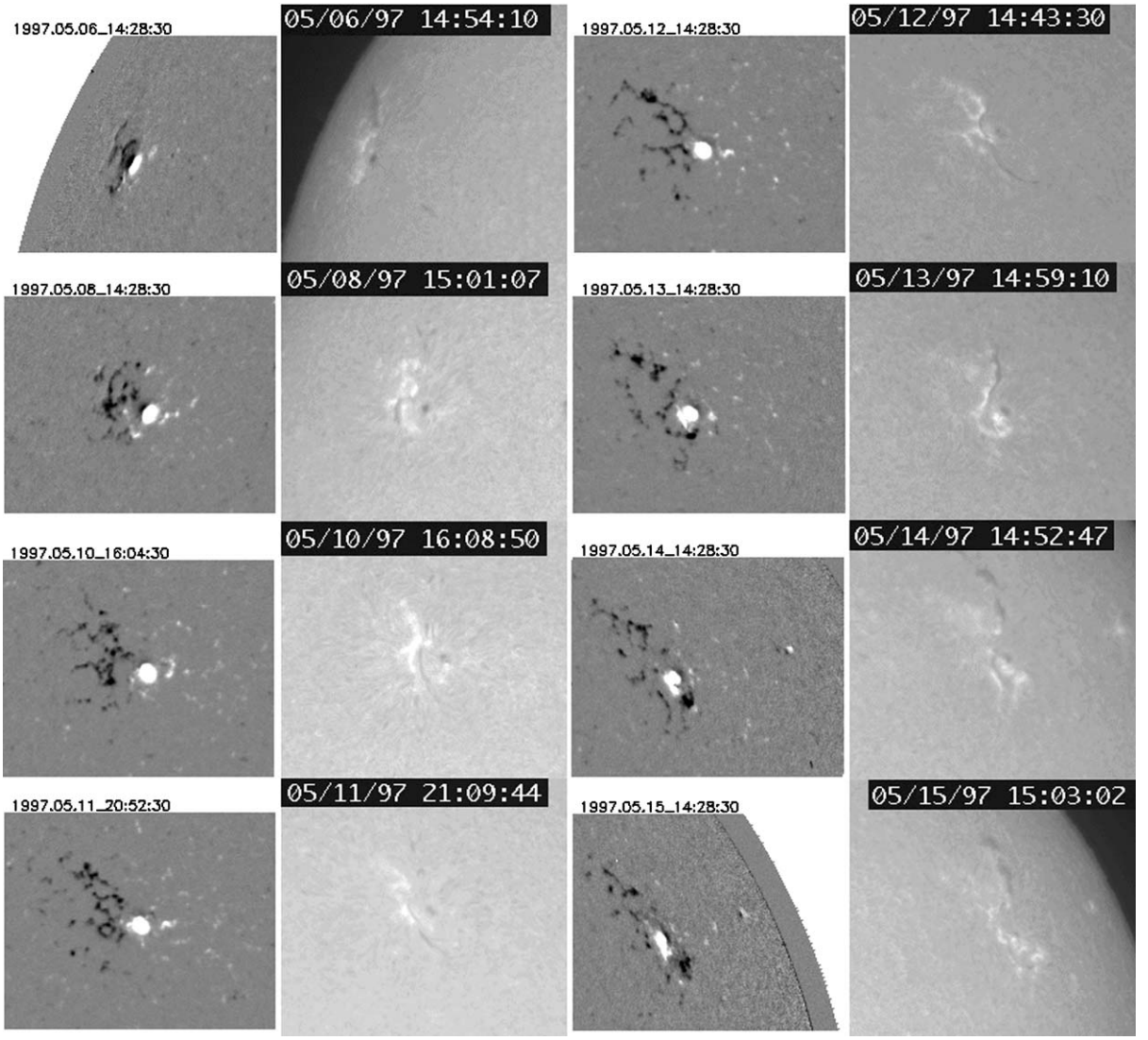

Fig. 3. A time-lapse sequence of the evolution of this active region from limb to limb as seen with the SOHO/MDI magnetograph and BBSO Hα images from May 6 to May 15, 1997.

or LCT is one method of inferring the velocities in the photosphere from sequences of images by cross correlating identifiable features or patterns. An inherent assumption of this method is that each pair of images only slightly differs from one another (Welsch et al., 2004).

One scheme of LCT finds proper motions of intensity features in successive images separated in time (Δt) by finding the shift that maximizes a cross-correlation function (November and Simon, 1988; Welsch et al., 2004). The shift measured in pixels reveals the motion that occurred over Δt. Multiplying the shift (in X or Y directions) by pixel size and dividing by Δt results in a velocity (Vx or Vy). For our analysis, we use a particular approach of LCT developed by Welsch et al. (2004). For each pixel in the image array, the image is multiplied by a Gaussian of width σ, centered at that pixel; the resulting image is cropped by chopping off the insignificant parts to increase computational speed; the cross-correlation function is computed between a pair of cropped images using standard fast-Fourier transform techniques; high-order interpolation is used to find the shifts in x and y that maximize the cross-correlation function to an accuracy of 0.1 pixel. The Vx and Vy velocity arrays from this method have the same dimension as the input images. Further detailed

descriptions of the method may be found in Welsch et al. (2004). The velocity from LCT applied to magnetograms is an apparent horizontal velocity which may include some false component if the solar magnetic fields are inclined to the solar surface and have a vertical velocity, see Welsch et al. (2004) for detailed discussions. For the purpose of this paper, this caveat will not affect our conclusions. The LCT routine was coded in IDL.

SOHO/MDI full disk magnetograms for the periods of interest are used in our study. The 96 min cadence images are available for all periods, and higher cadence images (one every 2 min) are available during part of September 1996 covering a CME event with a filament disappearance. We apply the LCT method to the magnetograms to infer the horizontal velocity field on the photosphere during the relevant periods. Observations are most suitable for the calculations when the selected region is near the disk center. We apply LCT with high cadence magnetograms from September 25 to 26 when the region 7978 is around the disk center, and the CME occurred on September 26. We use MDI 96 min magnetograms from May 9 to 13 for the LCT calculations on region 8038 surrounding the time of the May 12, 1997 CME.

First, we extract the region including the entire active region of interest from the full disk magnetogram images to obtain a sequence of active region magnetograms. The AR magnetograms are then co-aligned with the first image of a particular sequence to remove the shift between the entire frame, which may be due to solar rotation, satellite pointing, etc. These images are then grouped in pairs. With the high cadence data, each pair is chosen to be four hours apart for the LCT method in order for significant shift and the increment of each pair is 10 min in order to observe the temporal evolution. For example, the first pair includes one image at 16:25:30 UT and a second image at 20:25:30 UT, and the second pair includes one image at 16:35:30 UT and a second image at 20:35:30 UT, and so forth. The velocity resulting from the pair at 16:25:30 and 20:25:30 UT is considered to be the velocity at 18:25:30 UT. When there are bad or missing images, we exclude them, then we try

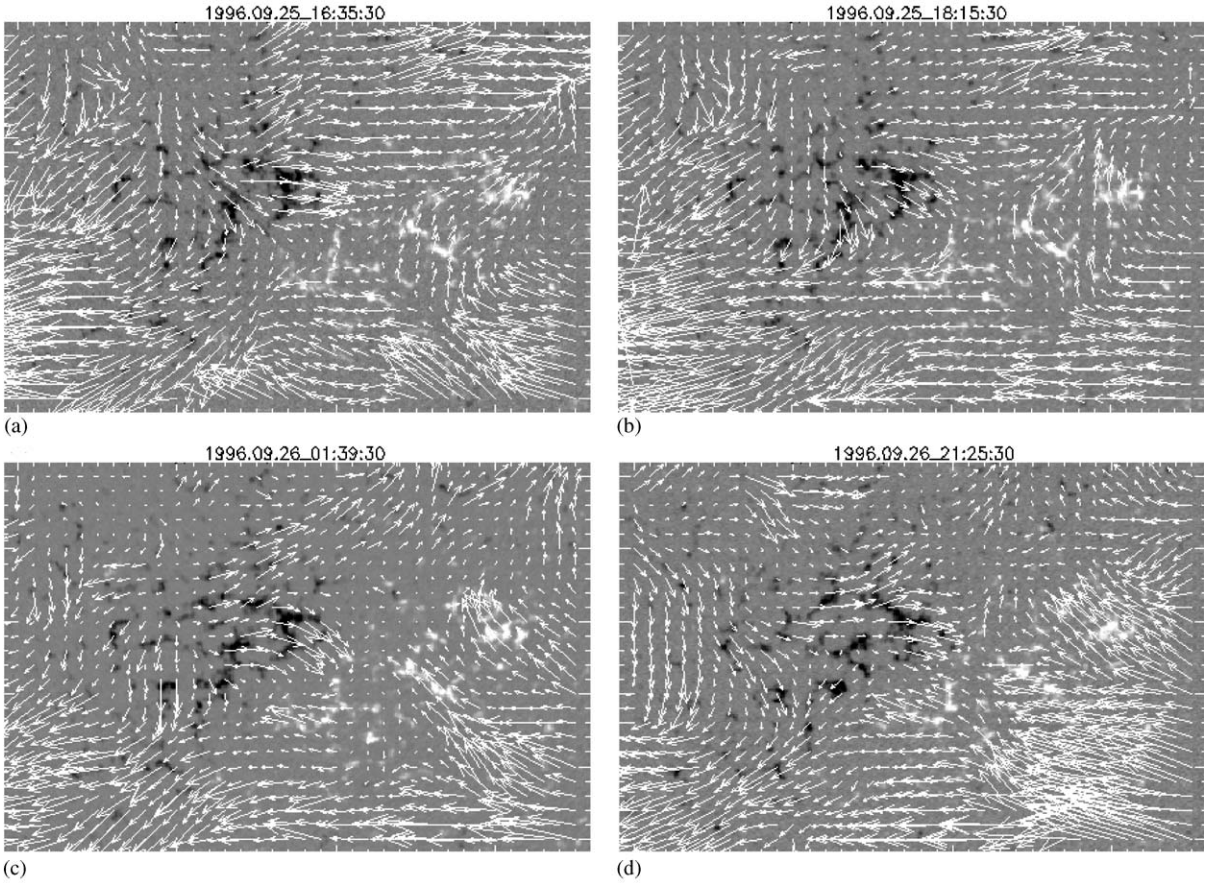

Fig. 4. The velocity field from LCT applied to a series of MDI magnetograms. From top to bottom are the results at 16:35 and 18:15 UT on September 25, and at 01:39 and 21:25 UT on September 26, 1996. Convergence towards the magnetic neutral line is apparent at all times.

to use images that keep the time separation as close as possible to the ones described here. With images of 96 min cadence, we pair up every other image that is 3 hr and 12 min apart and consider the velocity to be for the time between the pair. Each extracted AR magnetogram for the September 96 case has the size of 360 by 260 pixels, and for the May 97 case, 200 by 160 pixels. An MDI magnetogram has the pixel size of 1.95″ or $\sim 1409\,km^2$.

4. Results

4.1. September 96

From the LCT analysis on the September 25–26, 1996 MDI magnetograms, we obtained a series of velocity field results for every 10 min from about 14:30 UT on September 25 to 4:46 UT on September 26 (disk center was at $\sim$ 14:30 UT on September 24), and a movie animation (not shown) to visualize the field evolution. There was a data gap of about 17 h on September 26. The velocity field was thus obtained and a movie animation made covering 17:25–23:59 UT on September 26. Fig. 4 shows selected velocity field snapshots from this period as horizontal vectors on the photosphere superposed on a magnetogram from the period used to derive them. The spatial resolution of the vectors is the same as the input magnetogram images at about 1409 km, but reduced 10 times for visualization. The magnitude of the vectors ranges from 0 to ~ 0.2 km/s. The estimated error in these velocities is approximately 5% and was determined by applying a known velocity field to a magnetogram from the sequence to produce a 2nd false magnetogram. Applying LCT to this pair was used to determine the recovered velocity field. The difference between the assumed and recovered velocity fields results in an estimate of the error.

Our selected snapshots in Fig. 4 represent times before, during and after the eruption of active region 7978. It is apparent that the positive and negative magnetic fields converge toward the magnetic neutral line around the center of the region at all times. There are also flows that are not converging in other parts of the region; the roles of these in CME initiations are not clear at this early stage of the study. We will concentrate on the converging flows and shear flows, which have

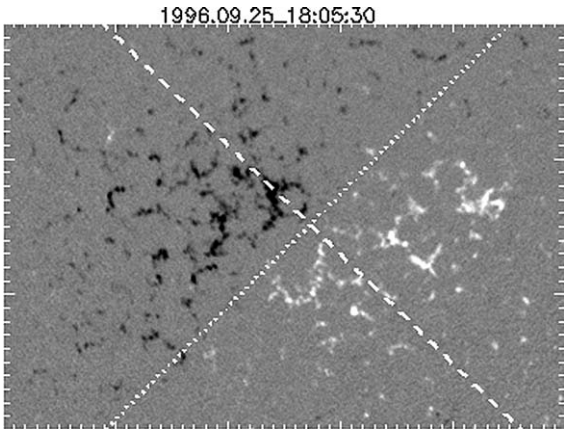

Fig. 5. On a magnetogram image of the active region at 18:05 UT on September 25, the approximate position of the magnetic neutral line of the center part of the active region is indicated by a dotted line. The dashed line is perpendicular to the neutral line and through the maximum converging flow region, along which we will make a cut of the velocity field and plot the component that is perpendicular to the neutral line V_{perp} and the one that is parallel to the neutral line V_{para} to investigate the converging flow and shear flow, respectively.

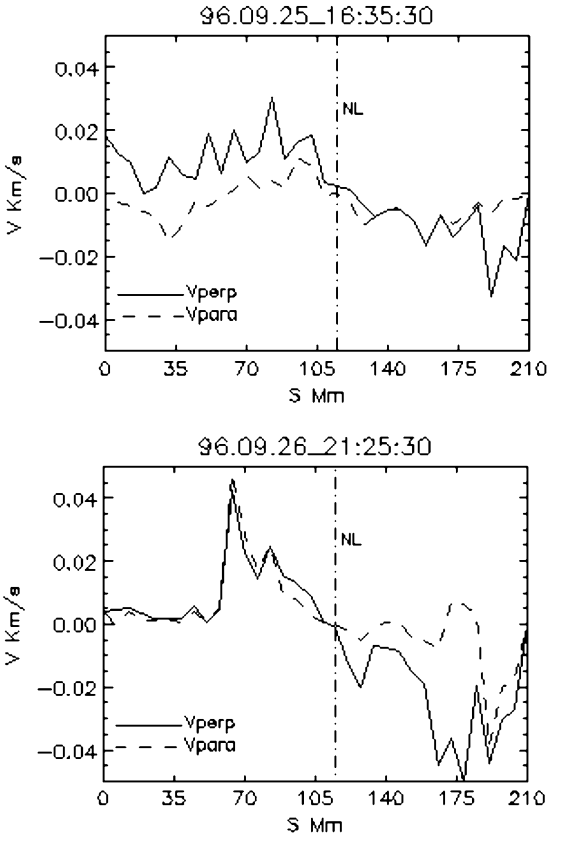

Fig. 6. Spatial profile of V_{perp} (perpendicular to the NL) along the dashed line in Fig. 5 is represented by the solid line. Dashed lines here represent the spatial profile of V_{para} (parallel to the NL). Dot-dashed lines represent the magnetic neutral line (NL) position of the decayed active region. V_{perp} and V_{para} profiles are shown for the first and last snapshots in Fig. 4. One may see converging flow towards the NL and shear flow along the NL (refer to the text for the direction definition of the flows).

been shown to play a role in initiating eruptions by a number of modeling studies discussed earlier in this paper. To quantify both the converging flow and shear flow and the associated velocity magnitudes, we make a cut through the field in the region with maximum converging flow along the dashed line in Fig. 5. The dotted line in Fig. 5 represents the approximate position of the magnetic neutral line of the center part of the decayed active region, while the dashed line is perpendicular to the neutral line and cut through the active region. Here we define V_{perp} as the velocity component perpendicular to the neutral line and V_{para} as the component parallel to the neutral line. The values of V_{perp} and V_{para} observed along the dashed line are used to generate the spatial profiles of the two velocity components across the active region, and samples at September 25 16:35 and 26 21:25 UT are given in Fig. 6. The dot-dashed line marks the position of the magnetic neutral line (NL). Positive V_{perp} means flow toward the lower-right corner perpendicular to the neutral line, and positive V_{para} means flow toward the upper-right corner along the neutral line. One can see discontinuities in the V_{perp} profile with converging flow from both side of the NL. The magnitude of V_{perp} is of the order of 0.02 km/s. One can also see discontinuities in V_{para} crossing the NL, which implies the existence of shear flows.

A series of the spatial profiles with 10 min cadence from September 25 16:35 to September 26 01:39 UT and from September 26 19:25 to 21:55 UT are stacked to give Fig. 7 to show the temporal evolution of the converging flow (top panel) and the shear flow (bottom panel). Each spatial profile is offset by 0.01 km/s from the previous one for the display, while the absolute scale of the velocity for each profile is preserved. The temporal order is from bottom to top as shown in the figure. The magnitude of the converging flow appears to be decreasing towards the time of the filament disappearance and the associated CME. Unfortunately, there was a data gap immediately after the time of the eruption. Results from data obtained about 17 h after the eruption shows an increased magnitude of the converging flow, but at a location slightly further away from the neutral line. As seen in the bottom panel, before the eruption there was a small shear flow near the neutral line, and the magnitude was slightly increasing towards the time of the eruption. After the eruption, a stronger shear flow magnitude similar to the converging flow appeared at the same time and same location, in particular in the negative polarity part of the active region.

We also calculated LCT results using 96 min MDI magnetograms for October 23 in the next solar rotation three days after a similar CME with a filament disappearance. Converging flow toward the magnetic neutral line is also observed (not shown). The magnitude of the converging flow in this related event period is of the same order at ~ 0.02 km/s.

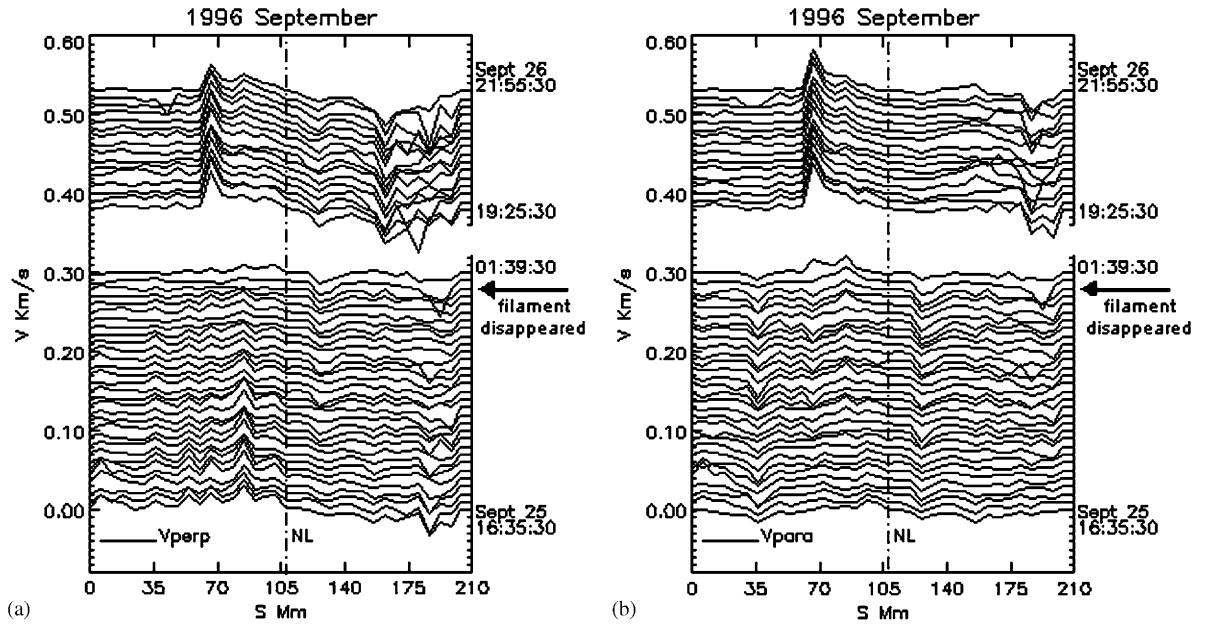

Fig. 7. A series of the spatial profiles with 10 min cadence from September 25 16:35 to 26 01:39 UT and from September 26 19:25 UT to 21:55 UT are stacked to show the temporal evolution of the converging flow (top panel) and the shear flow (bottom panel). Each spatial profile is offset by 0.01 km/s from the previous one for the display, while the absolute scale of the velocity for each profile is preserved. There was a data gap shortly after the eruption as shown.

4.2. May 97 event period

The LCT velocity field results from 96 min magnetograms for May 9 to 13 (disk center was at ~ 00:00 UT on May 11) have been reduced and a movie animation made to visualize the evolution. The converging flow appears to increase with time in the movie. Selected snapshots are presented in Fig. 8. Features of the velocity fields are qualitatively consistent during the few days. The upper panel of Fig. 8 shows one snapshot of the velocity field on May 11, 1997 shortly before the CME event. The lower panel of Fig. 8 gives the velocity field on May 12 soon after the flare and the halo CME. A clear convergence towards the neutral line of the active region is present at both times with the motion coming mostly from the negative polarity side (the positive polarity here is the sunspot). The spatial resolution of the vectors is the same as the input magnetogram images at about 1409 km, but reduced 5 times for visualization. The magnitude of the vectors ranges from 0 to ~ 2 km/s. The estimated error in these velocities is approximately 8%.

For this case, the short curved magnetic neutral line is approximately tangent to the vertical direction at the center of the active region (see Fig. 9). For the velocity component profiles, we simply make a horizontal cut through the region with the maximum converging flow across approximately the center of the sunspot (positive polarity) as shown in Fig. 9 with a dashed line. As before we designate the horizontal component of the velocity field V_{perp} (perpendicular to the magnetic neutral line), and the vertical component V_{para} (parallel to the magnetic neutral line). The values of V_{perp} and V_{para} along the dashed line in Fig. 9 are used to generate the spatial profiles in Fig. 10. Here positive V_{perp} means flow to the right, and positive V_{para} means flow upwards. One can also see discontinuities in V_{perp} indicating converging flows and in V_{para} indicating shear flows around the neutral line. The motions continue to be mostly in the negative polarity region. The magnitude of V_{perp} is on the order of 0.1 km/s, greater than the value from the previous case in September 1996. The magnitude of

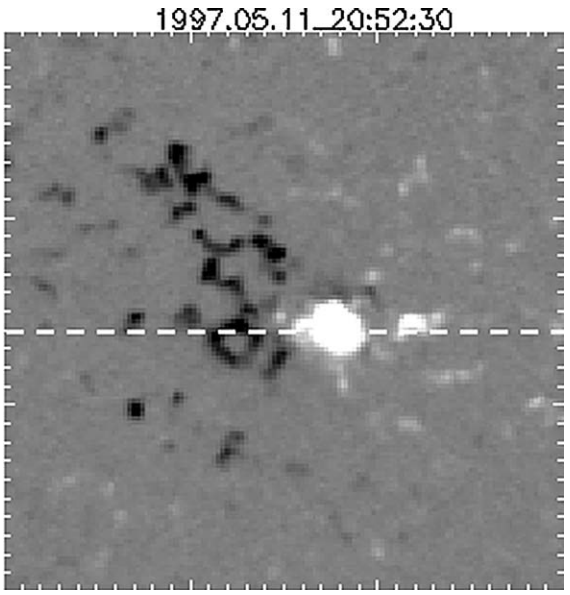

Fig. 9. For this case we will simply make a horizontal cut of the velocity field through region with the maximum converging flow near the center of the sunspot (positive polarity) that is effectively perpendicular with the vertical short neutral line as shown with the dashed line on the magnetogram at 20:52 UT on May 11, 1997. We will plot the horizontal component that is perpendicular to the neutral line V_{perp} and the vertical component that is parallel to the neutral line V_{para} to investigate the converging flow and shear flow, respectively.

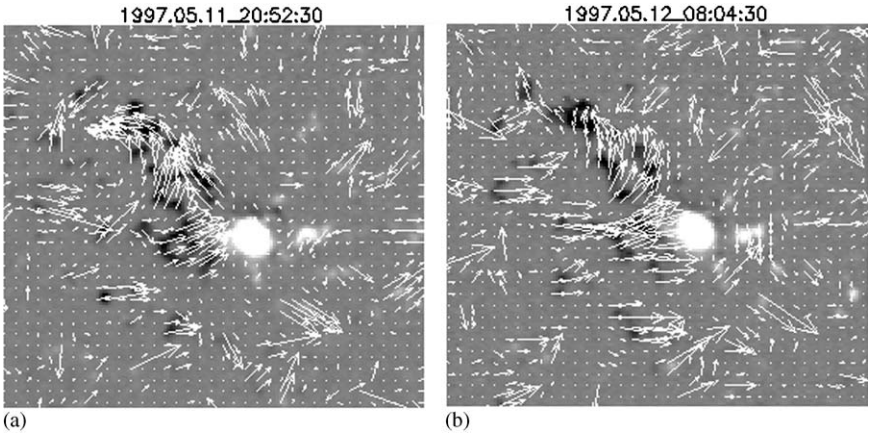

Fig. 8. The velocity field from LCT applied to MDI magnetograms on May 11, 1997 shortly before the event (upper panel) and May 12, 1997 soon after the event (lower panel). Convergence towards the magnetic neutral line is observed with the motion coming mostly from the negative polarity towards the sunspot (positive polarity) at both times.

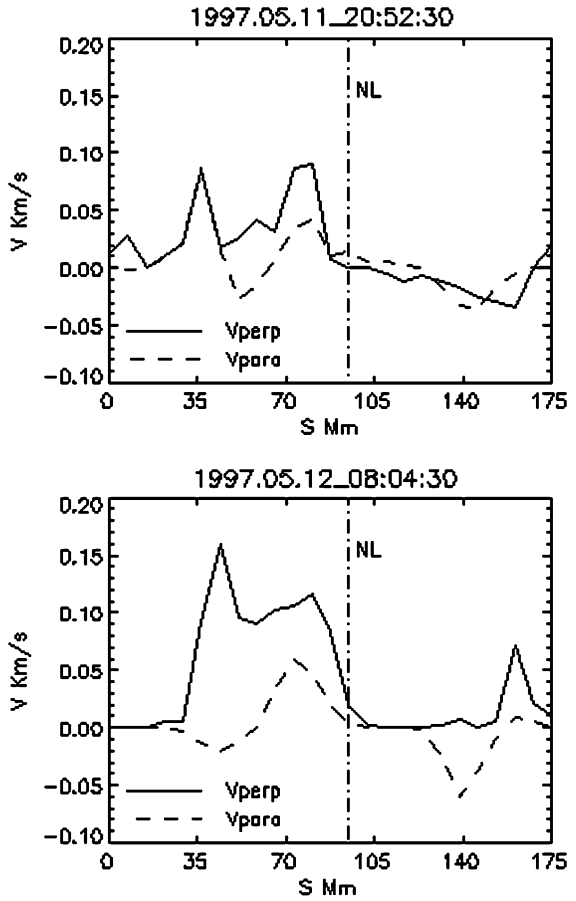

Fig. 10. The spatial profile of V_{perp} (perpendicular to the NL) along the dashed line in Fig. 5 is represented with solid lines. The dashed lines here represent the profile of V_{para} (parallel to the NL). Dot–dashed lines represent the vertical magnetic neutral line (NL) position of the center of the active region. V_{perp} and V_{para} profiles are shown for the two different times in Fig. 8 correspondingly. One may see converging flow towards the NL and shear flow along the NL (refer to the text for the direction definition of the flows).

V_{para} here is smaller than V_{perp}. A series of the profiles with 96 min cadence from 1997 May 9 01:40 to May 13 20:52 UT are stacked in Fig. 11 to investigate the temporal evolution of the converging flow (top panel) and shear flow (bottom panel). Each spatial profile is offset by 0.01 km/s from the previous one for the display, while the absolute scale of the velocity for each profile is preserved. The temporal order is from bottom to top as shown in the figure. The converging flow magnitude appears to increase towards the time of the flare and the CME, unlike the previous case in September 1996. The shear flow here shows a less consistent pattern and has no clear trend in temporal evolution.

5. Summary and conclusions

We have applied the LCT technique to several series of magnetograms showing the evolution of two types of active regions producing sequences of CME events. Our goal was to determine whether converging flows toward the magnetic neutral lines were present. One case involved a decayed active region and the other a young evolving active region with a sunspot. The former repeatedly produced CMEs with filament disappearances including one during the period selected for our study, and the later produced three homologous-looking CMEs with flares during its disk passage, including the well-known May 12, 1997 halo CME period also selected for our study.

Despite the very different characteristics of the regions, we found consistent converging flows toward the magnetic neutral line. The magnitude of the inferred converging velocity component for the decayed active region in September and October 1996 is of the order of 0.02 km/s, and for the active region in May 1997 it is much greater on the order of 0.1 km/s. Our observations support the assumptions of several theoretical and numerical models, which use such converging flows to initiate simulated filament and CME eruptions (e.g. Amari et al., 2003a, b; Linker et al., 2003; Roussev et al., 2003).

The temporal evolutions of the converging flows for the two cases exhibit different trends. For the September 1996 case with a decayed active region, the converging flow decreases in magnitude towards the eruption (filament disappearance and CME). For the May 1997 case with a young active region, the converging flow increases in magnitude towards the eruption (flare and CME). Further investigations of such trends in more cases are desirable.

In addition to supporting the general idea of flows converging on a magnetic neutral line as a possible CME-inducing mechanism, our results suggest how the velocities derived using LCT on scalar magnetograms may help define the boundary conditions for CME initiation in coronal MHD models. If routine LCT calculations performed on sequences of scalar magnetograms suggest convergent flows, they can identify potentially eruptive regions. While the observed horizontal components of the velocity derived here are not by themselves sufficient to drive an eruptive MHD simulation (e.g. Welsch et al., 2004), they can be used as parameters in a model simulation to evaluate the likelihood of eruption given particular assumptions about the vertical velocities. Indeed, vertical velocities in active regions derived from the more complete vector magnetogram, together with LCT techniques (Welsch et al., 2004) may show the greatest promise.

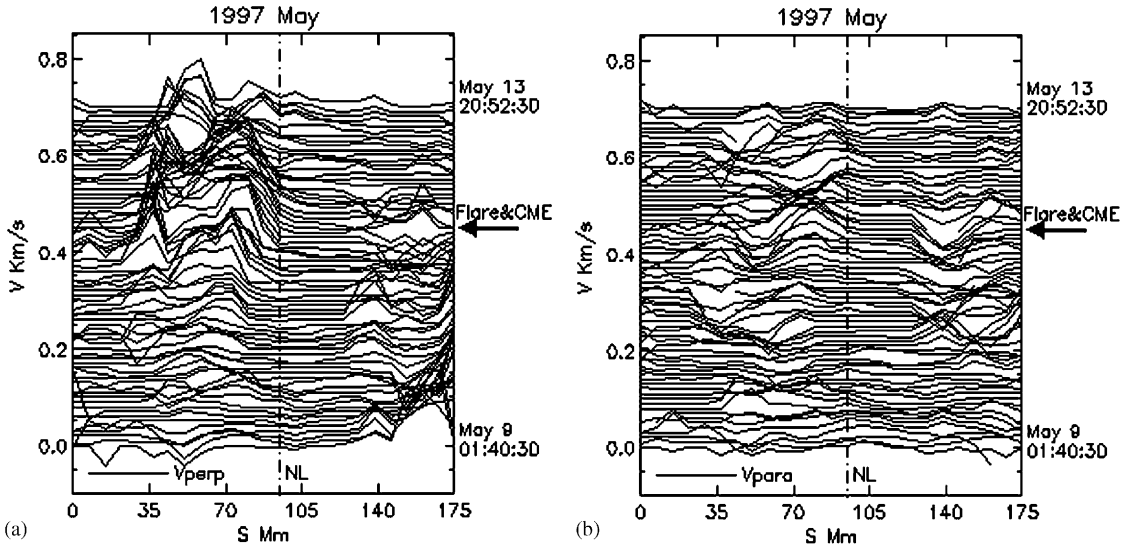

Fig. 11. A series of the profiles with 96 min cadence from 1997 May 9 01:40 to May 13 20:52 UT are stacked in Fig. 11 to investigate the temporal evolution of the converging flow (top panel) and shear flow (bottom panel). Each spatial profile is offset by 0.01 km/s from the previous one for the display, while the absolute scale of the velocity for each profile is preserved.

Acknowledgements

This material is based upon work supported in part by CISM, which is funded by the STC Program of the National Science Foundation under Agreement Number ATM-0120950, as well as the DoD/AFOSR "Solar MURI" grant "Understanding Magnetic Eruptions on the Sun and their Interplanetary Consequences" and NSF/Space Weather: Applications of GONG^{+} magnetograms. We thank the ESA and NASA-sponsored SOHO project, and especially the MDI investigators, for providing the data used in this study. We also thank the NJIT operators of Big Bear Solar Observatory for making their archive of Hα images publicly available.

References

Amari, T., Luciani, J.F., Aly, J.J., Micik, Z., Linker, J., 2003a. Coronal mass ejection: initiation, magnetic helicity and flux ropes. I. Boundary motion-driven evolution. Astrophysical Journal 585, 1073–1086.

Amari, T., Luciani, J.F., Aly, J.J., Micik, Z., Linker, J., 2003b. Coronal mass ejection: initiation, magnetic helicity, and flux ropes. II. Turbulent diffusion-driven evolution. Astrophysical Journal 595, 1231–1250.

Brown, D.S., Nightingale, R.W., Alexander, D., Schrijver, S.J., Metcalf, T.R, Shine, R.A., Title, A.M., Wolfson, C.J, 2003. Observations of rotating sunspots from trace. Solar Physics 216, 79–108.

Canfield, R.C., Hudson, H.S., McKenzie, D.E., 1999. Sigmoidal morphology and eruptive solar activity. Geophysical Research Letters 26 (6), 627.

Démoulin, P., Mandrini, C.H., van Driel-Gesztelyi, L., Thompson, B.J., Plunkett, S., Kövári, Zs., Aulanier, G., Young, A., 2002. What is the source of the magnetic helicity shed by CMEs? The long-term helicity budget of AR 7978. Astronomy & Astrophysics 382, 650–665.

Fan, Y., 2001. Nonlinear growth of the three-dimensional undular instability of a horizontal magnetic layer and the formation of arching flux tubes. Astrophysical Journal 546 (1), 509–527.

Fan, Y., Gibson, S.E., 2003. The emergence of a twisted magnetic flux tube into a preexisting coronal arcade. Astrophysical Journal 589 (2), L105–L108.

Feynman, J., Martin, S.F., 1995. The initiation of coronal mass ejections by newly emerging magnetic flux. Journal of Geophysical Research 100 (A3), 3355–3367.

Hudson, H.S., Labonte, B.J., Sterling, A.C., Watanabe, Te., 1998. NOAA 7978: The last best old-cycle region. In: Watanabe, T., Kosugi, T., Sterling, A.C. (Eds.), Observational Plasma Astrophysics: Five years of Yohkoh and Beyond. Kluwer Academic Publishers, Dordrecht, p. 37.

Linker, J.A., Lionello, R., Mikic, Z., Amari, T., 2001. Magnetohydrodynamic modeling of prominence formation within a helmet streamer. Journal of Geophysical Research 106 (A11), 25165–25176.

Linker, J.A., Mikic, Z., Lionello, R., Riley, P., Amari, T., Odstrcil, D., 2003. Flux cancellation and coronal mass ejections. Physics of Plasmas 10 (5), 1971.

Lionello, R., Mikic, Z., Linker, J., Amari, T., 2002. Magnetic field topology in prominences. Astrophysical Journal 581, 718–725.

Luhmann, J.G., Li, Y., Zhao, X., Yashiro, S., 2003. Coronal magnetic field context of simple CMEs inferred from global potential field models. Solar Physics 213 (2), 367–386.

Magara, T., 2001. Dynamics of emerging flux tubes in the sun. Astrophysical Journal 549, 608–628.

Magara, T., Longcope, D.W., 2001. Sigmoid structure of an emerging flux tube. Astrophysical Journal 559 (1), L55–L59.

November, L.J., Simon, G.W., 1988. Precise proper-motion measurement of solar granulation. Astrophysical Journal 333, 427–442.

Roussev, I.I., Sokolov, I.V., Forbes, T.G., Gombosi, T.I., Lee, M.A., Sakai, J.I., 2004. A numerical model of a coronal mass ejection: shock development with implications of the acceleration of GeV protons. Astrophysical Journal Letters, in press

Thompson, B.J., Plunkett, S.P., Gurman, J.B., Newmark, J.S., St. Cyr, O.C., Michels, D.J., 1998. SOHO/EIT observations of an Earth-directed coronal mass ejection on May 12, 1997. Geophysical Research Letters 25 (14), 2465.

Tokman, M., Bellan, P.M., 2002. Three-dimensional model of the structure and evolution of coronal mass ejections. Astrophysical Journal 567, 1202–1210.

Wang, Y.-M., 2001. On the relationship between $He_{II}\lambda 304$ prominences and the photospheric magnetic field. Astrophysical Journal 560, 456–465.

Webb, D.F., Lepping, R.P., Burlaga, L.F., Deforest, C.E., Larson, D.E., Martin, S.F., Plunkett, S.P., Rust, D.M., 2000. The origin and development of the May 1997 magnetic cloud. Journal of Geophysical Research 105 (A12), 27251–27260.

Welsch, B.T., Fisher, G.H., Abbett, W.P., Regnier, S., 2004. ILCT: recovering photospheric velocities from magnetograms by combining the induction equation with local correlation tracking. Astrophysical Journal, 610, 1148–1156.